

GRU^{spa}: Gated Recurrent Unit with Spatial Attention for Spatio-Temporal Disaggregation

Bin Han
bh193@uw.edu
University of Washington
Seattle, USA

Bill Howe
billhowe@uw.edu
University of Washington
Seattle, USA

ABSTRACT

Open data is frequently released spatially aggregated, usually to comply with privacy policies. But coarse, heterogeneous aggregations complicate learning and integration for downstream AI/ML systems. In this work, we consider models to disaggregate spatio-temporal data from a low-resolution, irregular partition (e.g., census tract) to a high-resolution, irregular partition (e.g., city block). We propose a model, **Gated Recurrent Unit with Spatial Attention (GRU^{spa})**, where spatial attention layers are integrated into the original Gated Recurrent Unit (GRU) model. The spatial attention layers capture spatial interactions among regions, while the gated recurrent module captures the temporal dependencies. Additionally, we utilize containment relationships between different geographic levels (e.g., when a given city block is wholly contained in a given census tract) to constrain the spatial attention layers. For situations where limited historical training data is available, we study transfer learning scenarios and show that a model pre-trained on one city variable can be fine-tuned for another city variable using only a few hundred samples. Evaluating these techniques on two mobility datasets, we find that GRU^{spa} provides a significant improvement over other neural models as well as typical heuristic methods, allowing us to synthesize realistic point data over small regions useful for training downstream models.

CCS CONCEPTS

• **Networks** → *Network experimentation; Network performance modeling*; • **Computing methodologies** → *Spatial and physical reasoning*; • **Applied computing**;

KEYWORDS

disaggregation, spatiotemporal prediction, attention, urban computing, synthetic data, transfer learning

ACM Reference Format:

Bin Han and Bill Howe. 2024. GRU^{spa}: Gated Recurrent Unit with Spatial Attention for Spatio-Temporal Disaggregation. In *Proceedings of ACM Conference (Conference'17)*. ACM, New York, NY, USA, 10 pages. <https://doi.org/10.1145/nnnnnnn.nnnnnnn>

Permission to make digital or hard copies of all or part of this work for personal or classroom use is granted without fee provided that copies are not made or distributed for profit or commercial advantage and that copies bear this notice and the full citation on the first page. Copyrights for components of this work owned by others than the author(s) must be honored. Abstracting with credit is permitted. To copy otherwise, or republish, to post on servers or to redistribute to lists, requires prior specific permission and/or a fee. Request permissions from permissions@acm.org.
Conference'17, July 2017, Washington, DC, USA

© 2024 Copyright held by the owner/author(s). Publication rights licensed to ACM.
ACM ISBN 978-x-xxxx-xxxx-x/YY/MM
<https://doi.org/10.1145/nnnnnnn.nnnnnnn>

1 INTRODUCTION

High-quality, longitudinal, and freely available urban data, coupled with advances in machine learning, improve our understanding and management of urban environments [13]. Over the last two decades, cities have increasingly released datasets publicly on the web, proactively, in response to transparency regulation. For example, in the US, all 50 states and the District of Columbia have passed some version of the federal Freedom of Information (FOI) Act. While this first wave of open data was driven by FOI laws and made national government data available primarily to journalists, lawyers, and activists, a second wave of open data, enabled by the advent of open source and web 2.0 technologies, was characterized by an attempt to make data “open by default” to civic technologists, government agencies, and corporations [45].

Open data affords study of urban dynamics [46, 51], but, with few exceptions [38, 54], models assume access to individual-level data, while privacy concerns motivate the release of aggregated data [12] such that aggregated data tends to be the norm in some fields [4, 22, 28]. Although aggregation can protect individual privacy [9, 14, 42] (without strong guarantees [3, 16]), it complicates integration of multiple datasets (e.g., aligning tract-level to block-level data) and destroys information useful for training. For example, demographers have studied disaggregation techniques to uncover local hotspots erased by tract-level aggregation [34]. The New York City (NYC) taxi open datasets serve as another notable example, widely used in spatio-temporal traffic forecasting literature. Much of the work has relied on NYC taxi data collected before June 2016, when individual-level records were accessible [13, 17, 31, 53]. Subsequently, taxi records have been released at aggregated taxi zone levels, forcing applications to rely on out-of-date pre-2016 data.

Motivated by these issues, we study the spatio-temporal disaggregation problem: to break down the aggregated urban data from a coarse, irregular spatial partitioning to a finer, irregular partitioning. The disaggregation problem has been studied in different domains. Spatial disaggregation methods in the demography literature tend to rely on heuristics: areal weighting, which assumes all variables are constant per unit area [7], and dasymetric mapping [7], which assumes sufficient auxiliary data is available to predict the target variable using linear methods. Disaggregation has also been considered in the machine learning literature, outside of the spatiotemporal context, where the goal is to learn individual-level models given group-level aggregated data [32, 54]. However, these approaches explicitly seek a model where the target variable at the individual level is determined *only* by its parent group’s features as opposed to learning from global patterns across groups. In a spatiotemporal context, any region may influence any other: traffic on the bridge can increase wait times in midtown, for instance.

In this paper, we evaluate neural architectures for the disaggregation problem. We proposed an overarching model, **Gated Recurrent Unit with Spatial Attention (GRU^{spa})**, where spatial attention layers are incorporated in the Gated Recurrent Unit (GRU) model. The spatial attention layers capture the convoluted spatial interactions among regions, while the gated recurrent module captures the temporal dependencies. Specifically, the spatial attention layers calculate attention scores between the coarse and fine geographic regions. To enhance learning efficiency and effectiveness, we use (but do not necessarily require, *containment*: each fine level region is entirely contained in a coarse level region. Such phenomenon is practically seen in political boundaries. Exploiting this property, we create binary containment maps to be used in the spatial attention layers, promoting the generation of coherent and consistent values across varying geographic resolutions. We conduct three experiments targeting at different disaggregation levels. Our results show that GRU^{spa} significantly enhances disaggregation performance and exhibits faster convergence compared to other neural models.

In addition to our primary disaggregation findings, we conduct two experiments to enhance the practicality and the utility of the disaggregation task: 1) *Transfer Learning*. We relax the assumption that temporal historical data is always available and consider pre-training on variable A then fine-tuning on variable B. Our results demonstrate the remarkable effectiveness of transfer learning, yielding competitive outcomes with only a minimal number of data points. 2) *Individual Points Synthesis*. We first quantitatively show that our disaggregated values have a similar distribution to the ground truth values over a set of small block regions, via mutual information and Kullback–Leibler (KL) divergence statistics. Then we qualitatively demonstrate that a simple sampling scheme can be used to generate a realistic individual-level of points. The synthesized individual data can be further processed and used in other downstream tasks. Overall, we make the following contributions:

- We propose an original model, GRU^{spa}, designed to disaggregate spatio-temporal data. The spatial attention layers model the spatial interactions while the gated recurrent module captures the temporal dependencies. By employing containment maps, our model is guided to produce coherent and consistent values across different geographic resolutions. On average, our model deliver an 2.2% improvement over the best baseline neural models (GRUs) and an 19.3% improvement over the best classical methods (historical ratio models). Additionally, GRU^{spa} converge faster than other neural models.
- We evaluate the proposed model on two real mobility datasets addressing the scenario of the same city, but different variables. Our experiments demonstrate that the proposed model can enhance performance over the best baseline neural models (GRUs) on both datasets (2.3% on taxi data and 2.1% on bikeshare data).
- We consider a transfer learning setting, under the assumption that sufficient training data is not always available to train a good neural model for every city variable. We show that in the same city, parameters learned from one variable can be used to make predictions on another variable, through fast fine-tuning with limited resources (1~2 hours v.s. 12 hours of pre-training), with competitive or sometimes even better performances.

- After disaggregating to small regions, we synthesize individual-level data via sampling. We show that synthesized points have similar distributions to the true values, evidenced by high mutual information (0.736) and low KL-divergence (0.058) statistics.

Our work is available at this repository for reproducibility ¹.

2 RELATED WORK

Spatial Disaggregation. Spatial disaggregation is frequently used in demography to infer individual records from spatially aggregated regions such as census data [35, 48], in applications including disease mapping [2] and vaccination coverage [43]. A popular heuristic is areal weighting (AW), which assumes the value per unit area is constant [11]. This method is common in practice due to its simplicity, general reliability, and ability to be computed from a single variable. Pycnophylactic interpolation (PI), first introduced by Tobler in 1979 [41], works similarly to areal weighting, but with a refinement to avoid discontinuities at the boundaries. PI distributes the values from source regions to target regions in an iterative manner, considering a weighted average of its nearest neighbors to avoid discontinuities while preserving the total count. Dasymetric mapping/interpolation/weighting (DM) approach is a family of methods that use the relationships between multiple variables to improve the estimated distribution. Unlike areal weighting, dasymetric mapping uses auxiliary information to generate a weighted distribution of source values onto the target regions. Recent methods incorporate machine learning approaches to model the relationships between auxiliary data and source values and determine the weights for disaggregation [33–35]. Sources of auxiliary information include satellite images [40], 3D building information [35], mobile phone usage data [8], terrain elevation and human settlement [33], and other variables more broadly available at high spatial and temporal resolution. Despite the popularity of dasymetric mapping methods in spatial disaggregation, there are several potential limitations of them [7]. They are wholly dependent on auxiliary variables, which are not always available (e.g., remote sensing images or land type data in population disaggregation tasks). Additionally, the performance of the model depends on the correlation between auxiliary data and source values, which may not be sufficiently high due to lack of relevant datasets or noisy measurements.

Learning From Aggregated Observations. In addition to the spatial disaggregation methods, it is also possible to learn individual level probabilistic models from aggregated data, without first decomposing aggregated data into individual instances. The problem is generally referred to as *learning from aggregated observations*, where supervision labels are given to sets of instances instead of individual instances, while the goal is still to make inferences on unseen individuals [22, 38, 54]. Zhang et al. [54] present a general probabilistic framework capable of accommodating a variety of aggregate observations for various tasks, such as classification and regression. They show that simple maximum likelihood solutions can be applied to various differentiable models such as deep neural networks and gradient boosting machines. Ma et al. [30] studied the problem of learning nonlinear dynamics from aggregated data, where individual trajectory data is not available. They proposed a

¹<https://github.com/BeanHam/2023-urban-disaggregation>

partial differential equation to describe the density evolution of aggregated data, which is subsequently combined with a Wasserstein generative adversarial network (WGAN) in the training process. Wei et al. [49] studies a more specific problem — classification from aggregate observations (CFAO), where the supervision is provided to groups of instances, instead of individual instances. They presented a novel universal method of CFAO, which generates unbiased estimators of the classification risk for arbitrary losses.

Spatio-Temporal Traffic Prediction. Spatiotemporal disaggregation can be cast as a prediction problem, for which neural methods have received significant attention. Traffic forecasting is a spatiotemporal prediction problem that is a building block for a number of mobility applications[18], such as trip planning (e.g., travel time estimation [24], route representation[27]) and resource optimization (e.g., dynamic fleet management [55]). Earlier work [23, 25, 52] used graph convolutional network (GCNs) to capture spatial interactions and sequential models such as Long-Short Term Memory (LSTMs) or Gated Recurrent Unit (GRUs), to model temporal dependencies. Later work [21, 56, 57] utilized spatial and/or temporal attention mechanisms to capture more complicated spatial and temporal dynamics and correlations. Recent work applies spatio-temporal transformers[10, 26, 50]. Spatio-temporal transformers have also been applied in other areas, such as visual tracking [50], trajectory prediction[5], and human action recognition[1].

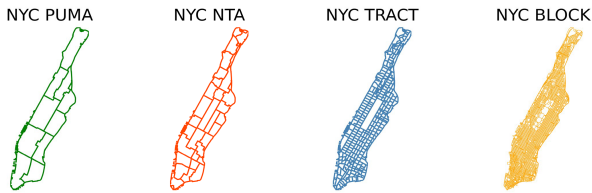


Figure 1: Four distinct geographic aggregation levels for the same NYC area. PUMA regions are the largest and most coarse. BLOCK regions are smallest and finest.

3 DATASETS

In our research, we use two mobility datasets — NYC taxi data and NYC bikeshare data. Each dataset contains individual-level records.

- **NYC Taxi Data:** NYC taxi trip data is collected from NYC Open Data portal² from 01/01/2016 to 06/30/2016. The raw data are presented in tabular format. Each record summarizes the information for one single taxi trip, which contains the longitude and latitude of the location of the trip start.
- **NYC Bikeshare Data:** NYC bikeshare data is collected from NYC DOT³ 01/01/2021 to 06/30/2021. Similar to the taxi data, the raw data are presented in tabular format. Each data point represents one bike trip, including the longitude and latitude of the location where the bike was unlocked.

These two datasets represent two examples of mobility behavior in the same built environment, affording comparisons under similar conditions. Moreover, these datasets afford transfer learning studies (e.g., training on taxi data and evaluating on bikeshare data) to address the situation where available data may be limited.

²<https://opendata.cityofnewyork.us/data/>

³<https://citibikenyc.com/system-datafrom>

We have restricted our experiments to the Manhattan region. We use four distinct pre-defined geographic levels offering varying levels of spatial resolution: Public Use Microdata Areas (PUMA), Neighborhood Tabulation Areas (NTA), Census Tracts (TRACT), and Census Blocks (BLOCK) (see Figure 1). We obtain the 2010 geographic boundaries for these levels from the NYC open data portal. Figure 1 shows the resolutions of four geographic levels.

3.1 Data Processing

Given a dataset of individual events ($lat, lon, time$), we construct raster representations (for CNN models) and vector (for other neural models) representations of spatiotemporal event data as follows:

Vector. We aggregate the event counts by hour and region for each of the four geographic levels. For example, there are 10 Public Use Microdata Areas (PUMA); a single hour of data is represented as simply a 10-element vector. The order of elements is arbitrary. More generally, the dataset is represented as $X \in \mathbb{R}^{N \times d}$, where N is the total number of hours, and d is the number of regions at a given geographic level (e.g., $d = 10$ for PUMA; $d=32$ for NTA).

Raster. We first define a 128×256 grid and plot the N regions at each geographic level. Each region has a corresponding value from the vector input — $X_n, n \in \{1, 2, \dots, N\}$, and the number of pixels located within the region — $C_n, n \in \{1, 2, \dots, N\}$. Then each pixel in each region takes the value of $\frac{X_n}{C_n}$. Pixels shared by more than one region are assigned to whichever region is smaller to avoid ambiguity. This representation captures the shape of, and spatial relationships between, individual regions and affords the use of convolutional layers to model local and non-local influences. The cost is that we lose information during translation since the raster representation does not represent region boundaries precisely, especially at BLOCK level.

We compute descriptive statistics, including means and standard deviations, for the counts of each dataset at different geographic levels. These statistics are shown in Table 1. For NYC Taxi data, the standard deviations are large demonstrating the significant variability in the count values between regions. For instance, Inwood in upper Manhattan has considerably fewer taxi rides compared to the more central areas of Manhattan. In the case of the NYC Bikeshare, we notice significantly smaller average values at the TRACT and BLOCK levels. This observation can be attributed to the distribution of the bikes, which may vary in frequency across different regions within the city. As a result, the average values of these datasets are lower at the more granular levels. For both datasets, we use the month of June as the test split, the month of May as the validation split, and the rest as training data.

Data	PUMA	NTA	TRACT	BLOCK
NYC Taxi	1443.01 (1776.03)	450.94 (689.16)	51.17 (73.32)	3.86 (8.03)
NYC Bikeshare	189.24 (279.28)	59.14 (97.86)	6.71 (13.09)	0.50 (2.51)

Table 1: Descriptive statistics of two datasets. The numbers are the average hourly taxi/bike counts per geographic region. The standard deviations are in the parenthesis.

4 MODELS

In this section, we describe the GRU^{spa} model composed of spatial attention layers within a GRU framework. We also describe the containment property that relates different levels of the aggregation hierarchy that can be used for supervision.

Notation We adopt the following notation:

- g^i for $i \in \{0, 1, \dots, G\}$ denotes a geographic aggregation level. The levels are labeled in ascending order in terms of number of regions, i.e., the lowest resolution is assigned 0 and the highest resolution is assigned G . In our experiments, the input is always the lowest resolution, e.g. PUMA. Therefore, it is assigned with the level g^0 . Level g^G has the largest number of regions, which is BLOCK. Level $(g^1, g^2, \dots, g^{G-1})$ are intermediate levels.
- $|g^i|$ denotes the number of regions at geographic level g^i . $|g^G|$ denotes the number of regions at the BLOCK level, which we use to normalize the loss terms. That is, the loss for all levels is expressed in average error per city block to afford direct comparisons across levels.
- $X^i \in \mathbb{R}^{N \times |g^i|}$ denotes the ground truth $N \times |g^i|$ vector at geographic level g^i assuming N total hours. We include a subscript $(n) \in [1, N]$ to indicate a single timestep $X_n^i \in \mathbb{R}^{|g^i|}$. To indicate a range of timesteps n to $n+T$, we will write $X_{n:n+T}^i$.
- $\hat{X}^i \in \mathbb{R}^{N \times |g^i|}$ denotes the predicted data at geographic level g^i assuming N total hours. We will indicate slices of this vector using the same subscript notation as with ground truth.

4.1 Containment Property

The geographic levels we use exhibit *containment*: each region at level g^i is wholly contained in a region at level g^{i-1} such that regions are hierarchical. This property tends to hold in political contexts. For example, one census tract comprises multiple census blocks. Assuming containment, we can identify a one-to-many map among the regions from any two geographic levels. Let $M^{i,j}, \forall j > i$ be a $|g^i| \times |g^j|$ binary matrix representing the containment relationship between geographic levels g^i and g^j . A value of 1 at position $M^{i,j}[c, r]$ indicates that region r at level g^j is contained in region c at level g^i . Figure 2(a) shows an example where three regions from level g^i at a single n th timestamp are split into six regions from level g^j . Figure 2(b) presents the corresponding containment map.

4.2 Spatial Attention (SA) Layer

Spatio-temporal transformers have been used in urban prediction tasks (§2). The spatial attention layer in the transformer block can capture complex spatial relationships among different regions to improve performance. In the disaggregation task, spatial attention is calculated across two different geographic levels (Figure 2(c)). A spatial attention head (SA_{head}) for the disaggregation task works as follows – Given one timestamp input $X_n^i \in \mathbb{R}^{|g^i|}$ from geographic level g^i , we first calculate the key, query, and value metrics:

$$Q = X_n^i W_Q \in \mathbb{R}^{|g^i|}, W_Q \in \mathbb{R}^{|g^i| \times |g^i|} \quad (1)$$

$$K = X_n^j W_K \in \mathbb{R}^{|g^j|}, W_K \in \mathbb{R}^{|g^i| \times |g^j|} \quad (2)$$

$$V = X_n^i W_V \in \mathbb{R}^{|g^i|}, W_V \in \mathbb{R}^{|g^i| \times |g^i|} \quad (3)$$

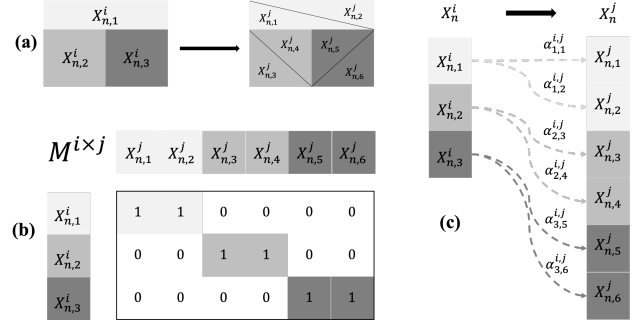


Figure 2: (a) Containment relationships between geographic level g^i and g^j . Each region from g^j is wholly contained in a region from g^i . (b) Binary containment map $M^{i,j}$ between geographic level g^i and g^j . (c) Spatial attention in disaggregation is calculated between two different geographic levels.

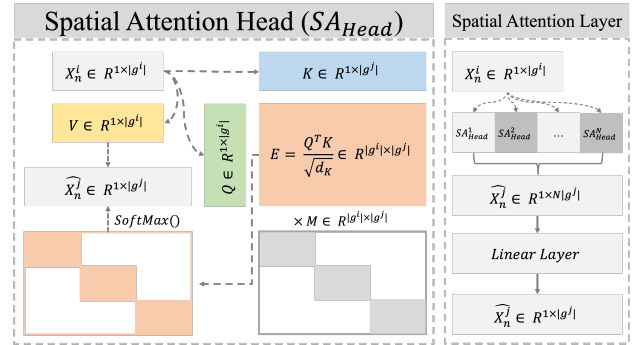


Figure 3: A spatial attention layer is composed with multiple spatial attention heads. Each spatial attention head calculates attention scores across regions from two different geographic levels. Including the containment map ensures the generation of coherent values across different resolutions.

Q and V have the same dimension as level g^i , while K has the dimension of the geographic level g^j . Then we attend the coarse region values to the finer region values by calculating the dot-product spatial attention. Additionally, we use the binary containment maps to force the attention to happen only among the connected regions:

$$Attention = \text{Softmax}(M^{i,j} \odot \frac{Q^T K}{\sqrt{|g^j|}}) \in \mathbb{R}^{|g^i| \times |g^j|} \quad (4)$$

The containment maps represent a constraint that child region values must sum to their parent's region value, ensuring coherent and consistent values across different geographic resolutions. The disaggregation output from a single spatial attention head is then calculated as:

$$SA_{Head}(Q, K, V) = V \cdot \text{Softmax}(M^{i,j} \odot \frac{Q^T K}{\sqrt{|g^j|}}) \in \mathbb{R}^{|g^j|} \quad (5)$$

A spatial attention (SA) layer is composed with multiple spatial attention heads SA_{Head} , enhancing the model capacity (Figure 3):

$$SA = \text{MultiHead}(Q, K, V) = \text{Concat}(h_1, h_2, \dots, h_N) W_O \quad (6)$$

$$h_i = SA_{Head}(Q_i, K_i, V_i)$$

The same calculation works with temporal inputs. Given T hours of input $X_{n:n+T}^i$ from geographic level g^i , we reshape the dimension $X_{n:n+T}^i \in \mathbb{R}^{T \times 1 \times |g^i|}$ and calculate spatial attention based on Eq (6).

In the typical spatial attention calculation [44], a residual connection layer is applied after the multi-head attention layer: $X_n^i + \text{MultiHead}(Q, K, V)$. In the disaggregation task, the input X_n^i and output $\text{MultiHead}(Q, K, V)$ have different dimensions, which cannot be added. Therefore, residual connection is not applicable. In our experiment, each SA layer uses eight SA_{Head} .

4.3 GRU^{spa}

The spatial attention layer only captures spatial dependencies across different geographic levels. The temporal information, which is also critical for spatio-temporal prediction tasks, is not represented except as a set of independent samples. Recent research has increasingly employed spatio-temporal transformers for spatio-temporal traffic forecasting, where a temporal transformer decoder follows the spatial transformer encoder to generate final predictions. These temporal attention layers capture the temporal dependencies in the input sequences. Temporal attention layers are typically preferred to conventional recurrent models due to their ability to learn long-distance dependencies and their efficient implementations in parallel settings. Unlike recurrent models, where information encoded at each time step is retained solely for the subsequent step and quickly diminishes in influence, attention layers calculate attention scores across the entire sequence concurrently, thereby promoting shared sequential information. However, GRU is still widely adopted in spatio-temporal prediction tasks [6, 29, 36, 47]. Additionally, our setting exhibits relatively short temporal lengths, and we find empirically that GRU outperforms a temporal transformer based model.

Let $X_{n:n+T}^i$ be T hours of input from geographic level g^i . Then for each element in the input sequence, a GRU layer computes:

$$\begin{aligned} r_t &= \sigma(X_t^i W_{xr} + h_{t-1} W_{hr} + b_r) \\ z_t &= \sigma(X_t^i W_{xz} + h_{t-1} W_{hz} + b_z) \\ n_t &= \tanh(X_t^i W_{xn} + (r_t \odot h_{t-1} W_{hn} + b_n)) \\ h_t &= z_t \odot h_{t-1} + (1 - z_t) \odot n_t \end{aligned}$$

where $X_t^i \subset X_{n:n+T}^i \in \mathbb{R}^{1 \times |g^i|}$ is the input at time t , h_{t-1} is the hidden state of the layer at time $t - 1$ or the initial hidden state at time 0. The dimensions of the parameters are: $W_{xr}, W_{xz}, W_{xn} \in \mathbb{R}^{|g^i| \times |g^j|}$, $W_{hr}, W_{hz}, W_{hn} \in \mathbb{R}^{|g^i| \times |g^j|}$, $b_r, b_z, b_n \in \mathbb{R}^{1 \times |g^j|}$. h_t is the new hidden state at time t , which is the hidden input for next time.

In the GRU model, $X_t^i W_{xr}$, $X_t^i W_{xz}$ and $X_t^i W_{xn}$ changes the spatial dimension from coarse level $|g^i|$ to finer level $|g^j|$. In our GRU^{spa} model, we replace the three matrix multiplication with spatial attention layers. Then GRU^{spa} is capable of modeling spatial and temporal dependencies concurrently. The calculation becomes:

$$\begin{aligned} r_t &= \sigma(SA_{xr} + h_{t-1} W_{hr} + b_r) \\ z_t &= \sigma(SA_{xz} + h_{t-1} W_{hz} + b_z) \\ n_t &= \tanh(SA_{xn} + (r_t \odot h_{t-1} W_{hn} + b_n)) \\ h_t &= z_t \odot h_{t-1} + (1 - z_t) \odot n_t \end{aligned}$$

where SA_{xr}, SA_{xz} and SA_{xn} are three separately trained spatial attention layers. We only use one GRU layer for our experiments.

4.4 Loss

We calculate ℓ_1 loss at the target disaggregation level. However, since ℓ_1 loss divides by the size of the vector, meaning that the ℓ_1 loss will have different units at each aggregation level. For example, the ℓ_1 loss at the TRACT level is in units of “events per TRACT region” while the ℓ_1 loss at the BLOCK level is in units of “events per BLOCK region”, leaving the two losses incomparable. Therefore, to meaningfully compare the losses at different target disaggregation level, we normalize all loss terms to be events-per-region at a selected aggregation level. In our experiments, we normalize to the BLOCK level to assist with interpretation: we consider taxi rides per city block as more familiar than taxi rides per PUMA region, for example. We use the following loss at the target level g^i :

$$\ell_1^i = \frac{1}{|g^G|} \sum |\hat{X}_n^i - X_n^i| \quad (7)$$

5 EXPERIMENTS

In this section, we describe the baseline models to compare against for the disaggregation task. Additionally, we describe the setup for the study of transfer learning and point synthesis.

5.1 Baseline Models

As our baseline, we test several heuristic-based disaggregation methods used commonly in the literature and in practice, as well as variants of more recent neural approaches:

- **Constant Weighting (CW)**: The event count for a region in the output is assumed to be $\frac{1}{N}$ of the count in the containing region in the input, where N is the number of output regions contained in the input region. That is, this heuristic assumes the events are uniformly distributed, regardless of size and shape of the region.
- **Areal Weighting (AW)**: The event count for an output region r contained in an input region c is assumed to be proportional to the fractional area of r in c . That is, $|r| = \frac{A(r)|c|}{A(c)}$, where $A(r)$ is the area of region r and $|c|$ is the event count in region c . That is, this heuristic assumes events are uniform per unit area.
- **Historical Ratios (HR)**: The event count of an output region r is assumed to be a fixed proportion of the count of an input region c . The fixed proportion is computed as the average proportion from all historical timesteps.
- **Feedforward Neural Network (FNN)**: The event count for an output region r is assumed to be a (non-linear) function of all input regions, not just the containing region. The function is modeled as a multi-layer feedforward neural network trained on historical data. This approach attempts to capture the inter-dependencies between regions. We use several fully-connected intermediate layers.
- **Convolutional Neural Network (CNN)**: The event count at each output region r is extracted from the raster representation at the output aggregation level (e.g., city blocks). That raster representation in turn is learned from the raster representation of the input aggregation level (e.g., PUMA) using a typical UNet

architecture[37]. This approach models the non-linear relationships between regions, while emphasizing local effects through convolutional layers.

- **Gated Recurrent Unit (GRU)**: Where FNN only models the spatial connections (by assuming that each timestep is an independent sample), GRU can capture temporal patterns. We chose $T=5$ as the temporal sequence length across all our experiments based on the study [13]. Otherwise, this model is similar in inputs and outputs to FNN. We use several intermediate GRU layers.
- **Spatio-Temporal Attention (STA)**: a model with spatial and temporal attention layers. In contrast to typical spatio-temporal transformers employing multiple attention layers, our experiments employ a single spatial attention layer and a single temporal layer for two reasons: 1) The inclusion of a single spatial and temporal attention layer already results in a larger model compared to our proposed GRU^{spa} (See Table 2). 2) Preliminary experiments indicate that adding more layers to **STA** detrimentally impacts performance.

We test three disaggregation tasks — from PUMA to NTA, TRACT and BLOCK level respectively. We also tested GRU^{spa} model without the containment maps as an ablation study. Batch size, learning rate, early stop tolerance are set to 32, $1e-4$, and 50 respectively. We use 1xNVIDIA T4 GPU, 16 GB RAM, x4 vCPUs, for each task.

Resolutions	FNN	GRU	STA	GRU^{spa}
PUMA -> NTA	1.4K	10K	47K	40K
PUMA -> TRACT	89K	750K	3.3M	2.2M
PUMA -> BLOCK	15M	128M	585M	377M

Table 2: Model sizes with respect to parameter counts.

5.2 Transfer Learning

As mentioned in §1, we do not always have access to sufficient historical data for training. In these cases, we can consider whether a model pre-trained on one variable can be used to make predictions for another variable. We can use our models in this transfer learning setting by training on, say, taxi data, then fine-tuning on a limited amount of bikeshare. This approach can significantly increase the value of open data, by allowing one dataset to be used in different applications. The idea is reasonable, given the interconnectedness of city dynamics as a complex system [15]: everything depends on everything else. Moreover, the main signals being learned by any model are influenced by the built environment, human activity, and population density patterns, all of which tend to be exhibited in any spatio-temporal dataset in the same domain.

5.3 Event Data Synthesis

While the BLOCK aggregation level is high-resolution (smaller than census tracts for example), they remain spatially aggregated and cannot be directly utilized by applications requiring individual point data[22, 38, 54]. Additionally, if we can synthesize individual taxi rides for NYC Taxi data after June 2016 given the aggregated taxi zone data, it would significantly enhance the utility of the datasets. A simple approach to synthesize points is to learn a high-resolution aggregation at BLOCK level, then randomly sample within these regions to generate individual points, considering the physical built-in environment (e.g., building, hotel etc.). If a region has k events,

we can sample k events within its boundaries. Quality control is important for the synthesized data. Quantitatively, we can compare the distributions of real and disaggregated values across a set of BLOCK regions. We consider two statistics to measure similarities: Mutual Information (MI) and KL-divergence. We also assess the distribution similarity qualitatively through visualization.

6 RESULTS

In this section, we present our experimental results that answer the following questions:

- (Q1) Do neural methods improve performance over popular heuristic methods? (Yes) (Section §6.1)
- (Q2) Does our proposed GRU^{spa} improve disaggregation performance relative to competing neural methods? (Yes) Does GRU^{spa} converge faster than competing methods? (Yes) (Section §6.2)
- (Q3) Can we fine-tune a disaggregation model trained on one variable and have it perform competitively on a different variable? (Yes) (Section §6.3)
- (Q4) Can disaggregation models synthesize realistic individual events from aggregated values? (Yes) (Section §6.4)

6.1 All Neural Methods Outperform Heuristics

Table 3 presents the errors of the disaggregation task using both heuristic and neural methods. We observe that 1) As the target disaggregation resolution increases, the error increases across all methods, as expected. Predicting city block dynamics from large regional aggregates is a difficult problem. 2) Popular heuristic-based disaggregation methods, such as CW and AW, are non-competitive across all resolutions and datasets. The underlying heuristics are reasonable but cannot capture the dynamics at higher resolution: The distribution of taxi rides and bikeshare trips follows human activity patterns, which are influenced by the built environment, temporal effects, and non-linear interactions between regions, all of which are inaccessible to simple heuristics. 3) HR significantly outperforms other heuristics, indicating that temporal patterns are generally predictive. However, HR still overlooks the non-linear temporal and spatial variations present in the data, limiting its overall accuracy. 4) Neural-based methods outperform all commonly used heuristics in nearly all disaggregation tasks. GRU models, in particular, outperform models that solely rely on spatial information. GRU emerges as the best-performing baseline model. CNN models exhibit worse performance than HR models when disaggregating from PUMA all the way to BLOCK resolution. Upon investigation, this performance discrepancy is attributable to the information loss that occurs during the conversion from vector inputs to the image representations expected by CNN models. Overall, the results show that neural models, especially GRU models, outperform heuristic-based approaches.

6.2 GRU^{spa} Improves Neural Results

From Table 3, we observe that our proposed GRU^{spa} has the best performance among five out of six tasks, delivering an 2.0% improvement over the best neural models on average, and 19.3% improvement over the best classical methods (HR) on average. The largest improvement is observed when we disaggregate from PUMA to

Dataset	Resolutions	CW	AW	HR	CNN	FNN	GRU	STA	GRU ^{spa} _{no_map}	GRU ^{spa}
NYC Taxi	PUMA → NTA	1.8295	1.4072	0.4652	0.3601	0.2299	0.2208	0.2608	<u>0.2125</u>	0.2108*
	PUMA → TRACT	1.8416	2.0651	0.9650	0.7297	0.5606	0.5492	0.6507	0.5565	<u>0.5494</u>
	PUMA → BLOCK	3.0947	2.9705	1.7609	1.5306	1.4381	1.4130	1.4350	<u>1.3904</u>	1.3770*
NYC Bikeshare	PUMA → NTA	0.3047	0.2071	0.1114	0.1012	0.0861	0.0843	0.0945	<u>0.0843</u>	0.0833*
	PUMA → TRACT	0.5304	0.5032	0.2726	0.2595	0.2489	0.2427	0.2418	0.2374	<u>0.2376*</u>
	PUMA → BLOCK	1.4392	1.3792	0.3972	0.4065	0.3741	0.3668	0.3618	<u>0.3599</u>	0.3559*

Table 3: Disaggregation results from traditional and neural-based methods. The unit of the error is count/(block * hour). Bold and underline numbers indicate the best and second result in the corresponding disaggregation task respectively. * indicates statistical significance test from bootstrap sampling. Our GRU^{spa} has the best performance among five out of six tasks.

BLOCK with NYC Taxi data — on average, GRU^{spa} reduces taxi count error per hour in the entire Manhattan region by 134 relative to the GRU model. For statistical significance tests, we use bootstrap sampling for 10,000 iterations [19, 39]: On each iteration, we sample the predictions, then calculate error and compute the proportion that are better than the baseline to provide an empirical estimate of the p-value. We use 0.05 as the significance level. With both the taxi and bikeshare dataset, GRU^{spa} consistently outperforms GRU with statistically significant improvement (other than NYC Taxi, PUMA to TRACT). Comparing STA with GRU and GRU^{spa}, we notice that STA models perform poorly on the taxi dataset, even worse than FNN models. With bikeshare data, STA models outperform GRU when disaggregating from PUMA to TRACT and BLOCK, and are less competitive than GRU^{spa}. Temporal attention is not effective and is incapable of producing consistent results compared with recurrent modeling unit in the disaggregation task. Although attention-based solutions are increasingly popular due to their success in NLP, we find that relatively short sequences and smaller capacity models can still motivate recurrent models.

Figure 4 shows the convergence plots of neural models on two datasets. We notice that other than the disaggregation from PUMA to BLOCK on NYC Bikeshare dataset, GRU^{spa} models always start with, and maintain, lower ℓ_1 error throughout training, thus converging faster than other models. One explanation is that the spatial attention layers in GRU^{spa} models are aware of the spatial structures due to the containment maps, thus producing better disaggregation results more efficiently.

Ablation Study — Effectiveness of Containment Maps: We conduct an ablation study to demonstrate the effectiveness of the containment maps. We run GRU^{spa} models on both datasets without the containment maps in the spatial attention layers. From Table 3, we observe that without the containment maps, the disaggregation results are usually worse than results with the maps. Although the improvement is typically modest, the convergence plots in Figure 4 show that GRU^{spa} models without maps converge slower than those with the maps, as evidenced by consistently higher error throughout the training. Our interpretation is that the containment maps provide "hints" during training, steering the learning toward the correct solutions (which always exhibit the containment property), thereby converging faster. Additionally, even without the containment maps, GRU^{spa} results are still better than GRU on five out of six tasks, indicating the effectiveness of the spatial attention layers, and suggesting that even if the containment property does not hold, these methods will be generally effective.

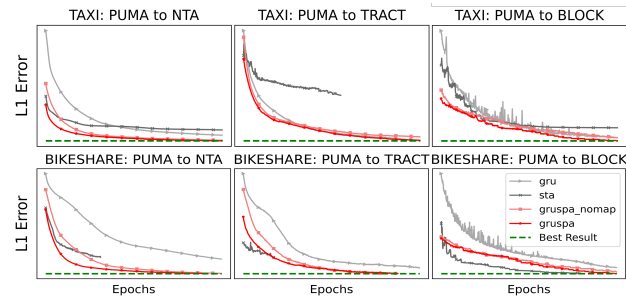


Figure 4: Convergence plots of neural models. Right three plots: show NYC Taxi dataset. Left three plots: Bottom rows shows NYC Bikeshare dataset. Red line represents our proposed GRU^{spa} model

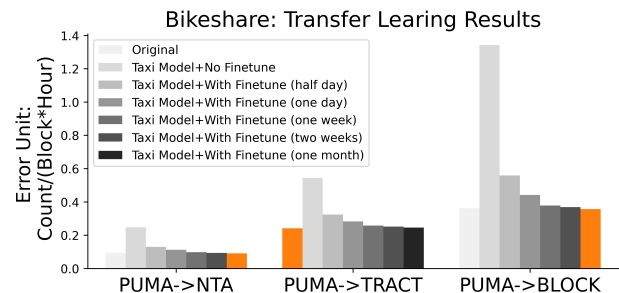


Figure 5: Transfer learning results on bikeshare dataset. The models are pre-trained with taxi data. The orange bar indicates the best performance for each disaggregation task.

6.3 Transfer Learning is Remarkably Effective

We trained GRU^{spa} models on NYC taxi data and evaluated on bikeshare in the same NYC domain. We fine-tuned with a half day (12 hour-long samples), one day (24), 4 days (96), one week (168 samples), and two weeks (336). Figure 5 shows the results: adding more fine-tuning samples enhances disaggregation performance. Surprisingly, fine-tuning with only one week of data achieves results comparable with, sometimes even better than, the specialized model trained from scratch with bikeshare data. Additionally, fine-tuning a pre-trained model significantly reduces the computational costs. This result has significant implications for practical settings: Training data is not uniformly available for all variables due to technical, privacy, and political effects. But because cities are complex systems, all variables are interdependent [15]. This result shows that pre-training can capture city dynamics resulting from the built

environment and human activity, and that those signals tend to be predictive for multiple variables. We envision developing a core model pre-trained with ample historical records, then fine-tuning for different tasks in the same city, analogous to a language model being fine-tuned for more specialized tasks.

6.4 Realistic Synthesis of Individual Events

To generate individual point data, we use our best performing model GRU^{spa} to disaggregate from PUMA to BLOCK with NYC taxi data. Then, we measure the mutual information and KL divergence (using Python implementations⁴⁵) between the distribution of disaggregated values and the original distribution in the same time period and region set. Then, for each BLOCK region with k taxi counts, we randomly draw k points within the region. We work with a set of block regions in Manhattan as shown in Figure 6. We draw samples from this set of regions for the on 12PM-1PM, 06/01/2016.

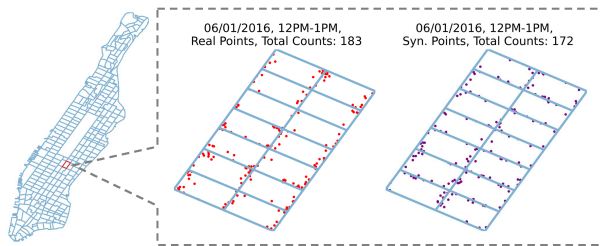


Figure 6: Synthetic individual-level taxi points. (Left) Randomly selected single tract region, containing multiple block regions. (Right) The distributions of real and synthesized taxis ride over the block regions are qualitatively similar.

The normalized MI scores is **0.7360**, smaller than 0.5, indicating that two distributions share more than half their information. The KL-divergence is **0.0582**. The low KL divergence indicates a reasonable approximation of the ground truth distribution using our disaggregated values. Qualitatively, Figure 6 depicts the distributions of both real and synthesized taxi location points within the region set from 12PM to 1PM. The model generated slightly smaller numbers of taxi rides compared to the real counts, with differences of 11 rides. While these differences are present, they are not significant compared with all taxi counts within the whole regions. In terms of the spatial distributions, the synthesized points capture the major clusters observed in the real taxi rides for both time periods, such as the clusters in the bottom left and center. This suggests that the synthesized points closely approximate the general patterns and trends present in the real data. On the other hand, the presence of discrepancies between the real and synthesized data points can have benefits, particularly in terms of privacy protection. As highlighted in the introduction, individual privacy is a significant motivator for *not* releasing individual-level data. A closely matching distribution could be used as the basis of a privacy attack. For instance, clusters within very small areas may reveal the address of frequent riders. We consider our methods as providing better control over the trade-offs between faithful distribution

⁴https://scikit-learn.org/stable/modules/generated/sklearn.metrics.normalized_mutual_info_score.html

⁵<https://docs.scipy.org/doc/scipy/reference/generated/scipy.stats.kstest.html>

and privacy (though without formal privacy guarantees, which are atypical for transportation data anyway).

7 DISCUSSION AND CONCLUSIONS

In this work, we synthesize high-resolution urban data by disaggregating low-resolution data. We considered neural models relative to popular heuristic methods in the literature. FNN and CNN models were able to capture spatial connections among different regions, while GRU models further incorporated temporal interdependence and produced better results.

We proposed a GRU^{spa} model, which replaces simple matrix multiplications with spatial attention layers in the GRU model. The spatial attention layers model the complex spatial interactions among regions, while the gated recurrent module captures temporal dependencies. To further capture spatial interactions, we enforce containment relationships between layers found in practice by multiplying the spatial attention result by a containment mask ensuring that child region counts always sum to parent region counts. Our experimental results on both taxi and bikeshare dataset consistently demonstrated the effectiveness of our proposed GRU^{spa} model, with statistically significant enhancements observed in almost all disaggregation tasks with faster convergence.

Since not all variables are available with significant training data, we considered the transferability of a model trained on one variable for predictions on another (in the same city). Surprisingly, with only a week of fine-tuning bikeshare data, the taxi model exhibited performance comparable to, sometimes better than, that of the bikeshare-only model. This result exposes that the underlying dynamics of human activity may appear in all variables observed from the same built environment, motivating new applications that integrate multiple data sources to overcome limited data availability [20]. We also showed that a simple samplign approach can synthesize individual events from aggregate data, exposing new opportunities for research.

There are some limitations to the study that we plan to address in future research: 1) we only considered the geographic levels for which containment holds. However, our spatial attention calculation is not limited by the containment property. We can still construct the containment maps even when a finer region overlap with more than one coarse regions. However, the extent to which these containment maps enhance learning effectiveness remains to be investigated in future studies. 2) Our current transfer learning experiments exclusively focus on scenarios where datasets originate from the same city and domain. This assumption implies shared geographic structures/grids and similar underlying dynamics. However, in practice, A) two variables could stem from different domains within the same city, resulting in varied underlying dynamics despite sharing the same city structure; B) transfer learning across cities, where the underlying dynamics may be different, is an important use case that we do not consider, and 3) We only investigated one set of regions to synthesize individual points for one time period. The spatial and temporal variances might impact the quality of the synthesized points. Additionally, we did not investigate whether the ability to synthesize individual events introduces privacy risk.

REFERENCES

- [1] Dasom Ahn, Sangwon Kim, Hyunsu Hong, and Byoung Chul Ko. 2023. STAR-Transformer: a spatio-temporal cross attention transformer for human action recognition. In *Proceedings of the IEEE/CVF Winter Conference on Applications of Computer Vision*. , 3330–3339.
- [2] Rohan Arambepola, Tim C. D. Lucas, Anita K. Nandi, Peter W. Gething, and Ewan Cameron. 2020. A simulation study of disaggregation regression for spatial disease mapping. *Statistics in Medicine* 41 (2020), 1–16.
- [3] Alissa Brauneck, Louisa Schmalhorst, Mohammad Mahdi Kazemi Majdabadi, Mohammad Bakhtiari, Uwe Völker, Jan Baumbach, Linda Baumbach, and Gabriele Buchholtz. 2023. Federated Machine Learning, Privacy-Enhancing Technologies, and Data Protection Laws in Medical Research: Scoping Review. *J Med Internet Res* 25 (30 Mar 2023), e41588. <https://doi.org/10.2196/41588>
- [4] J. Burrell, Tim Brooke, and R. Beckwith. 2004. Vineyard Computing: Sensor Networks in Agricultural Production. *Pervasive Computing, IEEE* 3 (02 2004), 38–45. <https://doi.org/10.1109/MPRV.2004.1269130>
- [5] Weihuang Chen, Fangfang Wang, and Hongbin Sun. 2021. S2tnet: Spatio-temporal transformer networks for trajectory prediction in autonomous driving. In *Asian Conference on Machine Learning*. PMLR. , 454–469.
- [6] Yibi Chen, Kenli Li, Chai Kiat Yeo, and Keqin Li. 2023. Traffic forecasting with graph spatial-temporal position recurrent network. *Neural Networks* 162 (2023), 340–349.
- [7] Alexis J. Comber and Wen Zeng. 2019. Spatial interpolation using areal features: A review of methods and opportunities using new forms of data with coded illustrations. *Geography Compass* (2019), .
- [8] Pierre Deville, Catherine Linard, Samuel Martin, Marius Gilbert, Forrest R. Stevens, Andrea E. Gaughan, Vincent D. Blondel, and Andrew J. Tatem. 2014. Dynamic population mapping using mobile phone data. *Proceedings of the National Academy of Sciences of the United States of America* 111, 45 (Sept. 2014), 15888–15893. <https://doi.org/10.1073/pnas.1408439111>
- [9] Zekeriya Erkin, Juan Ramon Troncoso-pastoriza, R.L. Legendijk, and Fernando Perez-Gonzalez. 2013. Privacy-preserving data aggregation in smart metering systems: an overview. *IEEE Signal Processing Magazine* 30, 2 (2013), 75–86. <https://doi.org/10.1109/MSP.2012.2228343>
- [10] Yuchen Fang, Fang Zhao, Yanjun Qin, Haiyong Luo, and Chenxing Wang. 2022. Learning all dynamics: Traffic forecasting via locality-aware spatio-temporal joint transformer. *IEEE Transactions on Intelligent Transportation Systems* 23, 12 (2022), 23433–23446.
- [11] M F Goodchild, Luc Anselin, and Uwe Deichmann. 1993. A Framework for the Areal Interpolation of Socioeconomic Data. *Environment and Planning A* 25 (1993), 383–397.
- [12] Ben Green, Gabe Cunningham, Ariel Ekblaw, Paul M. Kominers, Andrew Linzer, and Susan P. Crawford. 2017. Open Data Privacy: A risk-benefit, process-oriented approach to sharing and protecting municipal data. In . . .
- [13] Bin Han and Bill Howe. 2023. Adapting to Skew: Imputing Spatiotemporal Urban Data with 3D Partial Convolutions and Biased Masking. [arXiv:2301.04233 \[cs.CV\]](https://arxiv.org/abs/2301.04233)
- [14] W. He, X. Liu, H. Nguyen, K. Nahrstedt, and T. Abdelzaker. 2007. PDA: Privacy-Preserving Data Aggregation in Wireless Sensor Networks. In *IEEE INFOCOM 2007 - 26th IEEE International Conference on Computer Communications*. , 2045–2053. <https://doi.org/10.1109/INFCOM.2007.237>
- [15] Bill Howe, Jackson Brown, Bin Han, Bernease Herman, Nic Weber, An Yan, Sean Yang, and Yiwei Yang. 2022. Integrative urban AI to expand coverage, access, and equity of urban data. *The European Physical Journal Special Topics* 231 (04 2022). <https://doi.org/10.1140/epjs/s11734-022-00475-z>
- [16] Bin Jia, Xiaosong Zhang, Jiewen Liu, Yang Zhang, Ke Huang, and Yongquan Liang. 2022. Blockchain-Enabled Federated Learning Data Protection Aggregation Scheme With Differential Privacy and Homomorphic Encryption in IIoT. *IEEE Transactions on Industrial Informatics* 18, 6 (2022), 4049–4058. <https://doi.org/10.1109/TII.2021.3085960>
- [17] Yilun Jin, Kai Chen, and Qiang Yang. 2022. Selective cross-city transfer learning for traffic prediction via source city region re-weighting. In *Proceedings of the 28th ACM SIGKDD Conference on Knowledge Discovery and Data Mining*. , 731–741.
- [18] Yilun Jin, Kai Chen, and Qiang Yang. 2023. Transferable Graph Structure Learning for Graph-based Traffic Forecasting Across Cities. In *Proceedings of the 29th ACM SIGKDD Conference on Knowledge Discovery and Data Mining*. , 1032–1043.
- [19] Daniel Jurafsky and James Martin. 2008. *Speech and Language Processing: An Introduction to Natural Language Processing, Computational Linguistics, and Speech Recognition*. Vol. 2. . .
- [20] Aamod Khatiwada, Roece Shraga, Wolfgang Gatterbauer, and Renée J. Miller. 2022. Integrating Data Lake Tables. *Proc. VLDB Endow* 16, 4 (dec 2022), 932–945. <https://doi.org/10.14778/3574245.3574274>
- [21] Shiyong Lan, Yitong Ma, Weikang Huang, Wenwu Wang, Hongyu Yang, and Pyang Li. 2022. Dstagnn: Dynamic spatial-temporal aware graph neural network for traffic flow forecasting. In *International conference on machine learning*. PMLR, , 11906–11917.
- [22] Ho Chung Law, Dino Sejdinovic, Ewan Cameron, Tim Lucas, Seth Flaxman, Katherine Battle, and Kenji Fukumizu. 2018. Variational Learning on Aggregate Outputs with Gaussian Processes. In *Advances in Neural Information Processing Systems*, S. Bengio, H. Wallach, H. Larochelle, K. Grauman, N. Cesa-Bianchi, and R. Garnett (Eds.), Vol. 31. Curran Associates, Inc., . https://proceedings.neurips.cc/paper_files/paper/2018/file/24b43fb034a10d78bec71274033b4096-Paper.pdf
- [23] Mengzhang Li and Zhanxing Zhu. 2021. Spatial-temporal fusion graph neural networks for traffic flow forecasting. In *Proceedings of the AAAI conference on artificial intelligence*, Vol. 35. , 4189–4196.
- [24] Yaguang Li, Kun Fu, Zheng Wang, Cyrus Shahabi, Jieping Ye, and Yan Liu. 2018. Multi-task representation learning for travel time estimation. In *Proceedings of the 24th ACM SIGKDD international conference on knowledge discovery & data mining*. , 1695–1704.
- [25] Yaguang Li, Rose Yu, Cyrus Shahabi, and Yan Liu. 2017. Diffusion convolutional recurrent neural network: Data-driven traffic forecasting. *arXiv preprint arXiv:1707.01926* , (2017).
- [26] Hangchen Liu, Zheng Dong, Renhe Jiang, Jiewen Deng, Jinliang Deng, Quanjun Chen, and Xuan Song. 2023. Spatio-temporal adaptive embedding makes vanilla transformer sota for traffic forecasting. In *Proceedings of the 32nd ACM International Conference on Information and Knowledge Management*. , 4125–4129.
- [27] Hao Liu, Jindong Han, Yanjie Fu, Yanyan Li, Kai Chen, and Hui Xiong. 2023. Unified route representation learning for multi-modal transportation recommendation with spatiotemporal pre-training. *The VLDB Journal* 32, 2 (2023), 325–342.
- [28] Aurelie Lozano, Hongfei Li, Alexandru Niculescu-Mizil, Yan Liu, Claudia Perlich, Jonathan Hosking, and Naoki Abe. 2009. Spatial-temporal causal modeling for climate change attribution. In . *Proceedings of the ACM SIGKDD International Conference on Knowledge Discovery and Data Mining* , 587–596. <https://doi.org/10.1145/1557019.1557086>
- [29] Bin Lu, Xiaoying Gan, Weinan Zhang, Huaxiu Yao, Luoyi Fu, and Xinbing Wang. 2022. Spatio-Temporal Graph Few-Shot Learning with Cross-City Knowledge Transfer. In *Proceedings of the 28th ACM SIGKDD Conference on Knowledge Discovery and Data Mining*. , 1162–1172.
- [30] Shaojun Ma, Shu Liu, Hongyuan Zha, and Haomin Zhou. 2020. Learning Stochastic Behaviour of Aggregate Data. In *International Conference on Machine Learning*. . .
- [31] Jiqian Mo and Zhiguo Gong. 2022. Cross-City Multi-Granular Adaptive Transfer Learning for Traffic Flow Prediction. *IEEE Transactions on Knowledge and Data Engineering* , (2022), .
- [32] João Monteiro, Bruno Martins, Patricia Murrieta-Flores, and João M. Pires. 2019. Spatial Disaggregation of Historical Census Data Leveraging Multiple Sources of Ancillary Information. *ISPRS International Journal of Geo-Information* 8, 8 (2019), . <https://doi.org/10.3390/ijgi8080327>
- [33] João Monteiro, Bruno Martins, Patricia Murrieta-Flores, and João M. Pires. 2019. Spatial Disaggregation of Historical Census Data Leveraging Multiple Sources of Ancillary Information. *ISPRS International Journal of Geo-Information* 8, 8 (2019), . <https://doi.org/10.3390/ijgi8080327>
- [34] João Monteiro, Bruno Martins, and João Pires. 2018. A hybrid approach for the spatial disaggregation of socio-economic indicators. *International Journal of Data Science and Analytics* 5 (03 2018). <https://doi.org/10.1007/s41060-017-0080-z>
- [35] Yue Qiu, Xuesheng Zhao, Deqin Fan, and Songnian Li. 2019. Geospatial Disaggregation of Population Data in Supporting SDG Assessments: A Case Study from Deqing County, China. *ISPRS Int. J. Geo Inf.* 8 (2019), 356.
- [36] Qianqian Ren, Yang Li, and Yong Liu. 2023. Transformer-enhanced periodic temporal convolution network for long short-term traffic flow forecasting. *Expert Systems with Applications* 227 (2023), 120203.
- [37] Olaf Ronneberger, Philipp Fischer, and Thomas Brox. 2015. U-Net: Convolutional Networks for Biomedical Image Segmentation. *CoRR* abs/1505.04597 (2015), . [arXiv:1505.04597](https://arxiv.org/abs/1505.04597) <http://arxiv.org/abs/1505.04597>
- [38] Rahul Singh and Yongxin Chen. 2023. Learning Gaussian Hidden Markov Models From Aggregate Data. *IEEE Control Systems Letters* 7 (2023), 478–483. <https://doi.org/10.1109/LCSYS.2022.3187352>
- [39] Derek Sonderegger and Robert Buscaglia. 2020. *Introduction to Statistical Methodology, Second Edition*. . .
- [40] Forrest R. Stevens, Andrea E. Gaughan, Catherine Linard, and Andrew J. Tatem. 2015. Disaggregating Census Data for Population Mapping Using Random Forests with Remotely-Sensed and Ancillary Data. *PLOS ONE* 10, 2 (02 2015), 1–22. <https://doi.org/10.1371/journal.pone.0107042>
- [41] Waldo R. Tobler. 1979. Smooth Pycnophylactic Interpolation for Geographical Regions. *J. Amer. Statist. Assoc.* 74, 367 (1979), 519–530. <http://www.jstor.org/stable/2286968>
- [42] Ata Ullah, Muhammad Azeem, Humaira Ashraf, Abdulillah A. Alaboudi, Mamoona Humayun, and NZ Jhanjhi. 2021. Secure Healthcare Data Aggregation and Transmission in IoT—A Survey. *IEEE Access* 9 (2021), 16849–16865. <https://doi.org/10.1109/ACCESS.2021.3052850>
- [43] CE Utazi, Julia Thorley, V. Alegana, Mjgs Ferrari, Kristine Nilsen, Saki Takahashi, C. Jessica E. Metcalf, Justin Lessler, and AJ Tatem. 2018. A spatial regression model for the disaggregation of areal unit based data to high-resolution grids with application to vaccination coverage mapping. *Statistical Methods in Medical Research* 28 (2018), 3226–3241.

- [44] Ashish Vaswani, Noam Shazeer, Niki Parmar, Jakob Uszkoreit, Llion Jones, Aidan N Gomez, Lukasz Kaiser, and Illia Polosukhin. 2017. Attention is all you need. In *Advances in neural information processing systems*. 5998–6008.
- [45] Stefaan Verhulst, Andrew Young, Andrew Zahuranec, Susan Ariel Aaronson, Ania Calderon, and Matt Gee. 2020. The emergence of a third wave of open data. , (2020), .
- [46] Patrick Vogel, Torsten Greiser, and Dirk Christian Mattfeld. 2011. Understanding bike-sharing systems using data mining: Exploring activity patterns. *Procedia-Social and Behavioral Sciences* 20 (2011), 514–523.
- [47] Xiaoyang Wang, Yao Ma, Yiqi Wang, Wei Jin, Xin Wang, Jiliang Tang, Caiyan Jia, and Jian Yu. 2020. Traffic flow prediction via spatial temporal graph neural network. In *Proceedings of the web conference 2020*. , , 1082–1092.
- [48] N. A. Wardrop, W. C. Jochem, T. J. Birda, H. R. Chamberlaina, David J. Clarke, D. Kerra, Lars Bengtssona, S. Juranc, V. Seamand, and A. J. Tatema. 2018. Spatially disaggregated population estimates in the absence of national population and housing census data. In . , .
- [49] Zixi Wei, Lei Feng, Bo Han, Tongliang Liu, Gang Niu, Xiaofeng Zhu, and Heng Tao Shen. 2023. A Universal Unbiased Method for Classification from Aggregate Observations. arXiv:2306.11343 [cs.LG]
- [50] Bin Yan, Houwen Peng, Jianlong Fu, Dong Wang, and Huchuan Lu. 2021. Learning spatio-temporal transformer for visual tracking. In *Proceedings of the IEEE/CVF international conference on computer vision*. , , 10448–10457.
- [51] Haiyang Yu, Zhihai Wu, Shuqin Wang, Yunpeng Wang, and Xiaolei Ma. 2017. Spatiotemporal recurrent convolutional networks for traffic prediction in transportation networks. *Sensors* 17, 7 (2017), 1501.
- [52] Rose Yu, Yaguang Li, Cyrus Shahabi, Ugur Demiryurek, and Yan Liu. 2017. Deep learning: A generic approach for extreme condition traffic forecasting. In *Proceedings of the 2017 SIAM International Conference on Data Mining*. SIAM, , , 777–785.
- [53] Taoyi Zhang, Yubo Wang, and Zhicheng Wei. 2023. MCL-STGAT: Taxi demand forecasting using spatio-temporal graph attention network with Markov cluster algorithm. *Int. J. Innovative Comput. Inf. Control* 19, 4 (2023), 1251–1264.
- [54] Yivan Zhang, Nontawat Charoenphakdee, Zhenguo Wu, and Masashi Sugiyama. 2020. Learning from Aggregate Observations. In *Proceedings of the 34th International Conference on Neural Information Processing Systems (Vancouver, BC, Canada) (NIPS'20)*. Curran Associates Inc., Red Hook, NY, USA, Article 670, pages.
- [55] Bolong Zheng, Lingfeng Ming, Qi Hu, Zhipeng Lü, Guanfeng Liu, and Xiaofang Zhou. 2022. Supply-demand-aware deep reinforcement learning for dynamic fleet management. *ACM Transactions on Intelligent Systems and Technology (TIST)* 13, 3 (2022), 1–19.
- [56] Chuanpan Zheng, Xiaoliang Fan, Cheng Wang, and Jianzhong Qi. 2020. Gman: A graph multi-attention network for traffic prediction. In *Proceedings of the AAAI conference on artificial intelligence*, Vol. 34. , , 1234–1241.
- [57] Jiawei Zhu, Qiongjie Wang, Chao Tao, Hanhan Deng, Ling Zhao, and Haifeng Li. 2021. AST-GCN: Attribute-augmented spatiotemporal graph convolutional network for traffic forecasting. *IEEE Access* 9 (2021), 35973–35983.